DESY-17-048
28 April 2017

Running of the Charm-Quark Mass from HERA Deep-Inelastic Scattering Data

Abstract

Combined HERA data on charm production in deep-inelastic scattering have previously been used to determine the charm-quark running mass $m_c(m_c)$ in the $\overline{\rm MS}$ renormalisation scheme. Here, the same data are used as a function of the photon virtuality Q^2 to evaluate the charm-quark running mass at different scales to one-loop order, in the context of a next-to-leading order QCD analysis. The scale dependence of the mass is found to be consistent with QCD expectations.

A. Gizhko[9], A. Geiser[9], S. Moch[7], I. Abt[16], O. Behnke[9], A. Bertolin[19], J. Blümlein[26], D. Britzger[9], R. Brugnera[20], A. Buniatyan[2], P.J. Bussey[6], R. Carlin[20], A.M. Cooper-Sarkar[18], K. Daum[25], S. Dusini[19], E. Elsen[9,a3], L. Favart[1], J. Feltesse[5], B. Foster[8,a1], A. Garfagnini[20], M. Garzelli[7], J. Gayler[9], D. Haidt[9], J. Hladkỳ[21], A.W. Jung[10,a2], M. Kapichine[4], I.A. Korzhavina[15], B.B. Levchenko[15], K. Lipka[9], M. Lisovyi[9,a5], A. Longhin[19], S. Mikocki[12], Th. Naumann[26], G. Nowak[12], E. Paul[3], R. Plačakytė[7], K. Rabbertz[11], S. Schmitt[9], L.M. Shcheglova[15,a6], Z. Si[22], H. Spiesberger[14], L. Stanco[19], P. Truöl[27], T. Tymieniecka[24], A. Verbytskyi[16], K. Wichmann[9,b5], M. Wing[13,a4], A.F. Żarnecki[23], O. Zenaiev[9], Z. Zhang[17]

[1] Inter-University Institute for High Energies ULB-VUB, Brussels and Universiteit Antwerpen, Antwerpen, Belgium[b1]

[2] School of Physics and Astronomy, University of Birmingham, Birmingham, UK[b2]

[3] Physikalisches Institut der Universität Bonn, Bonn, Germany[b4]

[4] Joint Institute for Nuclear Research, Dubna, Russia

[5] Irfu/SPP, CE-Saclay, Gif-sur-Yvette, France

[6] School of Physics and Astronomy, University of Glasgow, Glasgow, United Kingdom[b2]

[7] II. Institute for Theoretical Physics, Hamburg University, Hamburg, Germany

[8] Institut für Experimentalphysik, Universität Hamburg, Hamburg, Germany[b6,b7]

[9] Deutsches Elektronen-Synchrotron DESY, Hamburg, Germany

[10] Kirchhoff-Institut für Physik, Universität Heidelberg, Heidelberg, Germany[b6]

[11] Karlsruher Institut für Technologie, Karlsruhe, Germany

[12] The Henryk Niewodniczanski Institute of Nuclear Physics, Polish Academy of Sciences, Krakow, Poland[b9]
[13] Physics and Astronomy Department, University College London, London, United Kingdom[b2]
[14] PRISMA Cluster of Excellence, Institut fur Physik, Johannes Gutenberg-Universität, Mainz, Germany, and Centre for Theoretical and Mathematical Physics and Department of Physics, University of Cape Town, Rondebosch 7700, South Africa
[15] Lomonosov Moscow State University, Skobeltsyn Institute of Nuclear Physics, Moscow, Russia[b8]
[16] Max-Planck-Institut für Physik, München, Germany
[17] LAL, Université Paris-Sud, CNRS/IN2P3, Orsay, France
[18] Department of Physics, University of Oxford, Oxford, United Kingdom[b2]
[19] INFN Padova, Padova, Italy[b3]
[20] Dipartimento di Fisica e Astronomia dell' Università and INFN, Padova, Italy[b3]
[21] Institute of Physics, Academy of Sciences of the Czech Republic, Praha, Czech Republic[b10]
[22] Shandong University, Jinan, Shandong Province, P.R. China
[23] Faculty of Physics, University of Warsaw, Warsaw, Poland
[24] National Centre for Nuclear Research, Warsaw, Poland
[25] Fachbereich C, Universität Wuppertal, Wuppertal, Germany
[26] Deutsches Elektronen-Synchrotron DESY, Zeuthen, Germany
[27] Physik-Institut der Universität Zürich, Zürich, Switzerland[b11]

[a1] Alexander von Humboldt Professor; also at DESY and University of Oxford
[a2] Now at Fermilab, Chicago, USA, and Purdue University, West Lafayette, USA
[a3] Now at CERN, Geneva, Switzerland
[a4] Also supported by DESY and the Alexander von Humboldt Foundation
[a5] Now at Physikalisches Institut, Universität Heidelberg, Germany
[a6] Also at University of Bristol, UK.

[b1] Supported by FNRS-FWO-Vlaanderen, IISN-IIKW and IWT and by Interuniversity Attraction Poles Programme, Belgian Science Policy
[b2] Supported by the UK Science and Technology Facilities Council
[b3] Supported by the Italian National Institute for Nuclear Physics (INFN)
[b4] Supported by the German Federal Ministry for Education and Research (BMBF), under contract No. 05 H09PDF
[b5] Supported by the Alexander von Humboldt Foundation
[b6] Supported by the Bundesministerium für Bildung und Forschung, FRG, under contract number 05H09GUF
[b7] Supported by the SFB 676 of the Deutsche Forschungsgemeinschaft (DFG)
[b8] Partially Supported by RF Presidential grant NSh-7989.2016.2
[b9] Partially Supported by Polish Ministry of Science and Higher Education, grant DPN/N168/DESY/2009
[b10] Supported by the Ministry of Education of the Czech Republic under the project INGO-LG14033
[b11] Supported by the Swiss National Science Foundation

1 Introduction

The Standard Model of particle physics is based on Quantum Field Theory, which can provide predictions that rely on a perturbative approach. In the $\overline{\text{MS}}$ renormalisation scheme of perturbative quantum chromodynamics (pQCD), the values of all basic QCD parameters depend on the scale μ at which they are evaluated. The most prominent example is the scale dependence, i.e. running, of the strong coupling constant α_s, a by now well established property of pQCD. It has, for example, been determined from measurements of hadronic event shapes or jet production at e^+e^- colliders [1, 2], and from measurements of jet production at HERA [3], Tevatron [4] and LHC [5].

The scale dependence of the mass m_Q of a heavy quark in the $\overline{\text{MS}}$ scheme can likewise be evaluated perturbatively, using the renormalisation group equation

$$\mu^2 \frac{d}{d\mu^2} m_Q(\mu) \;=\; m_Q(\mu)\, \gamma_{m_Q}(\alpha_s) \;, \tag{1}$$

which is governed by the mass anomalous dimension $\gamma_{m_Q}(\alpha_s)$ known up to five-loop order [6] in perturbation theory. The running of the $\overline{\text{MS}}$ beauty-quark mass has already been successfully investigated from measurements at the LEP e^+e^- collider [7]. Heavy-flavour production in deep-inelastic scattering (DIS) at HERA is particularly sensitive to heavy-quark pair production at the kinematic threshold. A recent determination of the beauty-quark mass $m_b(m_b)$ [8] by the ZEUS experiment at HERA was reinterpreted as a measurement of $m_b(\mu = 2m_b)$ using the solution of Eq. (1) at one loop. The comparison [9–11] of this result with the measurements from LEP and the PDG world average [12, 13] shows consistency with the expected running of the beauty-quark mass.

An explicit investigation of the running of the charm-quark mass has not been performed yet. Combined HERA measurements [14] on charm production in deep-inelastic scattering have already been used for several determinations of the charm-quark mass $m_c(\mu = m_c)$ in the $\overline{\text{MS}}$ renormalisation scheme [14–18]. Figure 1 shows the measured reduced cross section for charm production [14] as a function of the Bjorken variable x_{Bj} in 12 bins of photon virtuality Q^2 in the range $2.5\ \text{GeV}^2 < Q^2 < 2000\ \text{GeV}^2$. In this paper, these data are used to investigate the running of the charm-quark mass with the same treatment of the uncertainties of the combination as in Ref. [14]. The fixed flavour number scheme (FFNS) is used at next-to-leading order (NLO) with $n_f = 3$ active flavours. This scheme gives a very good description of the charm data [14, 19], as shown in Fig. 1. Calculations of next-to-next-to-leading order corrections with massive coefficient functions [18, 19] have not yet been completed, and are therefore not used in this paper.

2 Principle of the $m_c(\mu)$ determination

The theoretical reduced cross section for charm production is obtained from a convolution of charm-production matrix elements with appropriate parton density functions (PDFs). The latter are obtained from inclusive DIS cross sections, which include a charm contribution. Thus both, matrix elements and PDFs, depend on the value of the charm-quark mass. The scale dependence of the charm-quark mass is evaluated by subdividing the charm cross-section data [14] into several subsets corresponding to different individual scales, as indicated by different rows in

Fig. 1. In contrast, in the evaluation of the PDFs, data spanning a large scale range such as the inclusive HERA DIS data [20, 21] must be used in order to get significant PDF constraints. A subdivision into individual scale ranges is thus not possible for the PDF determination. On the other hand, it has been established that, apart from the strong constraint which the charm measurements impose on the charm-quark mass [14], their influence on a combined PDF fit of both inclusive and charm data is small [21]. Therefore, the PDFs extracted from inclusive DIS can be used for investigations of charm-quark properties, provided that the same charm-quark mass is used throughout, recognising that thereby some correlation between the mass and PDF extractions is induced. The influence of this correlation on the determination of the charm-quark mass running is minimised as described in section 4.

To obtain the charm-quark mass at different scales, the charm data are subdivided into six kinematic intervals according to the virtuality of the exchanged photon. Each measurement in a given range in Q^2, as listed in Table 1 and shown in Fig. 1, is performed with charm data originating from collisions at a typical scale of $\mu = \sqrt{Q^2 + 4m_c^2}$. The actual scale used for each interval is defined according to

$$\log \mu = \left\langle \log \left(\sqrt{Q^2 + 4m_c^2} \right) \right\rangle , \tag{2}$$

where the brackets indicate the logarithmic average of the considered range. The resulting value for each Q^2 range is also listed in Table 1.

Technically, a value of $m_c(m_c)$ is extracted separately from a fit to each interval. The value of $m_c(m_c)$ is obtained assuming the running of both α_s and m_c as predicted by QCD. To that end, Eq. (1) is solved using the one-loop dependence on the scale μ, as relevant in a NLO calculation, as

$$m_Q(\mu) \; = \; m_Q(m_Q) \times \left(\frac{\alpha_s(\mu)}{\alpha_s(m_Q)} \right)^{c_0} , \tag{3}$$

where $c_0 = 4/(11 - 2n_f/3) = 4/9$ as appropriate for QCD with $n_f = 3$ for the number of light quark flavours. Equation (3) is used to evaluate the mass running in all results of this work.

Expanded and truncated to leading order in powers of α_s, this can also be expressed in the form (not used here)

$$m_Q(\mu) = m_Q(m_Q) \left(1 + \frac{\alpha_s(\mu)}{\pi} \log \left(\frac{\mu^2}{m_Q^2} \right) + O(\alpha_s^2) \right) . \tag{4}$$

This illustrates that the scale dependence is logarithmic and justifies the logarithmic average in Eq. (2).

According to Eq. (3) the mass has actually been determined at the scale μ, and was extrapolated to the scale m_c when expressed as $m_c(m_c)$. If each determination of $m_c(m_c)$ is reinterpreted in terms of a value of $m_c(\mu)$ using Eq. (3), the mass determinations are reverted to their unextrapolated value, and the effect of the initial assumption of QCD running on the interpretation of their value is minimised for the final result.

3 QCD predictions and systematic uncertainties

QCD predictions for the reduced charm cross sections are obtained at NLO in pQCD ($O(\alpha_s^2)$) using the OPENQCDRAD package [22] as available in HERAFitter[1] [20, 23]. These predictions are based on the ABM implementation [24] of charm cross-section calculations in the

[1]Recently renamed xFitter.

3-flavour FFNS. The renormalisation and factorisation scales are always taken to be identical. In the calculations, the same settings and parametrisations are chosen as those used for the earlier measurement of $m_c(m_c)$ [14]. In addition, scale variations were applied as in Ref. [15]. For all explicit calculations of charm-quark mass running, an implementation of the one-loop formula [25], Eq. (3), is used, which is consistent with that used implicitly in OPENQCDRAD.

These predictions are fitted to the data. The fit uncertainty $\delta_{\rm fit}^{\rm exp}$ is determined by applying the criterion $\triangle\chi^2 = 1$ with the same formalism as in Ref. [14]. It contains the experimental uncertainties, the extrapolation uncertainties and the uncertainties of the default PDF parametrisation. In addition, the result has uncertainties attributed to the choices of extra model parameters, additional variations of the PDF parametrisation and uncertainties on the perturbative QCD parameters as listed in terms of δ_1 to δ_7 below.

The following additional parameters are used in the calculations, presented with the variations performed to estimate their systematic uncertainties

- δ_1: **$\overline{\rm MS}$ running mass of the beauty quark**, $m_b(m_b) = 4.75$ GeV, varied within the range $m_b(m_b) = 4.3$ GeV to $m_b(m_b) = 5.0$ GeV, to be consistent with [14];
- δ_2: **strong coupling constant** $\alpha_s^{n_f=3,\rm NLO}(M_Z) = 0.105 \pm 0.002$, corresponding to $\alpha_s^{n_f=5,\rm NLO}(M_Z) = 0.116 \pm 0.002$, as in [14];
- δ_3: **strangeness suppression factor** $f_s = 0.31$, varied within the range $f_s = 0.23$ to $f_s = 0.38$, as in [14];
- δ_4: **evolution starting scale** $Q_0^2 = 1.4$ GeV^2, varied to $Q_0^2 = 1.9$ GeV^2, as in [14];
- δ_5: **minimum Q^2 of inclusive data in the fit** $Q^2_{\rm min}$. For the PDF extraction, the minimum Q^2 of the inclusive data was set to $Q^2_{\rm min} = 3.5$ GeV^2 and varied to $Q^2_{\rm min} = 5$ GeV^2, as in [14];
- δ_6: **the parametrisation of the proton structure** is described by a series of FFNS variants of the HERAPDF1.0 PDF set [20] at NLO, evaluated for the respective charm-quark mass, for $\alpha_s^{n_f=3,\rm NLO}(M_Z) = 0.105 \pm 0.002$, consistent with δ_2.

  The additional PDF parametrisation uncertainties are calculated according to the HERAPDF1.0 prescription [20], by freeing three extra PDF parameters D_{u_v}, $D_{\bar{D}}$ and $D_{\bar{U}}$ in the fit;
- δ_7: **renormalisation and factorisation scales** $\mu_f = \mu_r = \sqrt{Q^2 + 4m_Q^2(m_Q)} = \mu$, varied simultaneously up (upper value) or down (lower value) by a factor of two for the massive quark (charm and beauty) parts of the calculation, as in [15].

The numerical values for each bin are shown in Table 2. The dominant uncertainties are those arising from $\delta_{\rm fit}^{\rm exp}$, followed by those from the scale variations δ_7.

4 Results

In order to minimise the correlated contribution from inclusive data to the charm-mass determinations, and in particular from the implicit charm-mass scale dependence therein, a set of

PDFs in the 3-flavour FFNS is extracted from a QCD fit to inclusive DIS HERA data [20]. This extraction uses exactly the same setup as that used in a previous publication [14], but allows for different charm-quark masses. The charm-quark mass as a function of scale is then extracted from a fit to the charm data only. When this analysis was originally performed [10, 11], the inclusive HERA II DIS data [21] were not yet available. The use of the earlier inclusive data [20] has been retained for several reasons. Firstly, all systematic uncertainties can be treated exactly as in the corresponding previous global $m_c(m_c)$ determination [14]. Secondly, the newer and more precise inclusive data are more strongly sensitive [17] to the assumed charm-quark mass and its running than the earlier inclusive data. This is actually counterproductive for the purpose of this paper in which the cross-correlations to the inclusive data, which cannot be subdivided into scale intervals, need to be minimised. Thirdly, the uncertainties on the determination of charm-quark mass running arising from the PDF uncertainties are already small (Table 2) compared to other uncertainties. For the purpose of this paper, the conceptual advantage of minimising the mass-related correlations between the charm and inclusive data sets therefore outweighs the potential gain from a higher PDF precision.

For each charm-quark mass hypothesis, predictions for the reduced charm cross sections are obtained using the corresponding PDF and are compared to one of the six subsets of the charm data listed in Table 1 and shown in Fig. 1. The $\overline{\text{MS}}$ running mass of the charm quark is varied within the range $m_c(m_c) = 1$ GeV to $m_c(m_c) = 1.5$ GeV in several steps. The χ^2 distribution of this comparison is used to extract the value of the charm-quark mass $m_c(m_c)$. An example of such a distribution for the first Q^2 interval is shown in Fig. 2, together with a parabolic fit. The minimum yields the measured charm-quark mass, while the fit uncertainty is obtained from $\Delta\chi^2 = 1$. The corresponding distributions for the other intervals can be found in Ref. [10]. A global fit to the complete charm data set for $m_c(m_c) = 1.26$ GeV, the central value obtained from the earlier global $m_c(m_c)$ analysis [14], is shown as a curve in Fig. 1 for comparison. The data are well described.

The values of $m_c(m_c)$ extracted for each of the subsets of charm data are shown in Fig. 3 and listed in Table 1 as a function of the corresponding scale μ, together with their uncertainties. The breakdown of the uncertainties into individual sources is summarised in Table 2. The values of $m_c(m_c)$ determined in the different subsets agree well within uncertainties with each other, with the value from the global analysis quoted above, and with the independent PDG world average[2] of 1.275 ± 0.025 GeV [12].

In order to test the stability of the $m_c(m_c)$ determination, the default analysis procedure is cross-checked with an alternative method. For each Q^2 interval a simultaneous PDF fit of the charm data from this interval and the full inclusive DIS data is performed. From the total χ^2 obtained by these fits, the χ^2 of the corresponding fits to the inclusive data only, is subtracted. These differences are then used for the determination of $m_c(m_c)$ by a χ^2 scan in the same way as for the standard procedure. Despite the more direct cross-correlation of the χ^2 from the charm sample with that from the inclusive sample in this method, the difference between the results of both methods is found to be negligible [10], i.e. smaller than the width of the line in Fig. 2. This indicates that the residual effect of the cross-correlation is small.

In the final step, the values of $m_c(m_c)$ are consistently translated back to $m_c(\mu)$ assuming the running of α_s and m_c as predicted by the QCD framework (Eq. 3). The resulting values of $m_c(\mu)$ are included in Table 1. The fractional contributions of the uncertainties for the individual

[2]The PDG2012 [12] value is used since it does not yet contain the result from [14] in the average, and is thus an independent value. The latest PDG2016 [13] value only differs very slightly from it.

sources (before the translation) are the same as those for $m_c(m_c)$ as listed in Table 2, with the exception of the scale-variation uncertainties δ_7 as discussed below.

In Fig. 4, the resulting scale dependence of $m_c(\mu)$ is shown together with the world average of $m_c(m_c)$ and the expectation for the evolution of $m_c(\mu)$ within the NLO QCD framework. The data are well described by the theoretical expectations. The running of the charm-quark mass as a function of the scale μ is clearly visible, if the independent PDG point obtained mainly from low scale QCD lattice calculations is included.

No scale variations are shown in Fig. 4. In addition to the scale uncertainties, δ_7, extracted from the fit, these would correspond to a variation in scale of the horizontal axis of the figure and/or a shift of the points along the expected scale-dependence curve, which are difficult to represent graphically. Furthermore, they are strongly correlated point by point, such that the shape of the distribution will stay essentially unchanged. In any case it is clear from Fig. 3 that their effect is not dominant.

Overall, this result is a nontrivial consistency check of the charm-quark mass running. It is conceptually similar to the procedure of extracting the running of $\alpha_s(\mu)$ from jet production at different transverse energy scales [3–5] or at different e^+e^- centre-of-mass energies [1, 2].

5 Conclusions

The running of the charm-quark mass $m_c(\mu)$ in the $\overline{\text{MS}}$ scheme is evaluated for the first time, using the combined reduced-cross-section charm data from HERA. It is found to be consistent with the expectation from QCD. Within the limited scale range of each subset of the charm data used for the determination of $m_c(\mu)$, the running of the charm-quark mass is implicitly assumed as part of the QCD theory input. Therefore this determination is not fully unbiased. However, the implicit bias of each individual $m_c(\mu)$ value is much smaller than the bias of the earlier extractions of a single $m_c(m_c)$ value from the complete data set. Furthermore, the PDG value of $m_c(m_c) = 1.275 \pm 0.025$ GeV indicated in Figs. 3 and 4 is mainly obtained from lattice gauge theory and time-like processes at scales in the vicinity of the charm-quark mass, at which its value is displayed. Therefore the comparison to this independent value is an important verification of the running of m_c, one of the basic features of QCD, at the same level as earlier evaluations of the running of m_b or of the running of α_s.

Acknowledgements

Part of this work was carried out within the scope of the PROSA, ZEUS and H1 Collaborations.

References

[1] O. Biebel, Phys. Rept. **340** (2001) 165; and references therein.
J. Schieck *et al.* [JADE Collaboration], Eur. Phys. J. **C73** (2013) 2332 [arXiv:1205.3714].
S. Bethke *et al.* [JADE Collaboration], Eur. Phys. J. **C64** (2009) 351 [arXiv:0810.1389].

[2] G. Abbiendi *et al.* [OPAL Collaboration], Eur. Phys. J. **C71** (2011) 1733 [arXiv:1101.1470].
G. Dissertori *et al.*, JHEP **0908** (2009) 036 [arXiv:0906.3436].

[3] S. Chekanov *et al.* [ZEUS Collaboration], Eur. Phys. J. **C44** (2005) 183 [hep-ex/0502007].
F.D. Aaron *et al.* [H1 Collaboration], Eur. Phys. J. **C65** (2010) 363 [arXiv:0904.3870].
F.D. Aaron *et al.* [H1 Collaboration], Eur. Phys. J. **C67** (2010) 1 [arXiv:0911.5678].
H. Abramowicz *et al.* [ZEUS Collaboration], Nucl. Phys. **B864** (2012) 1 [arXiv:1205.6153].
V. Andreev *et al.* [H1 Collaboration], Eur. Phys. J. **C77** (2017) 215 [arXiv:1611.03421].

[4] V.M. Abazov *et al.* [D0 Collaboration], Phys. Rev. **D80** (2009) 111107 [arXiv:0911.2710].
V.M. Abazov *et al.* [D0 Collaboration], Phys. Lett. **B718** (2012) 56 [arXiv:1207.4957].

[5] S. Chatrchyan *et al.* [CMS Collaboration], Eur. Phys. J. **C73** (2013) 2604 [arXiv:1304.7498].
V. Khachatryan *et al.* [CMS Collaboration], Eur. Phys. J. **C75** (2015) 186 [arXiv:1412.1633].
V. Khachatryan *et al.* [CMS Collaboration], Eur. Phys. J. **C75** (2015) 288 [arXiv:1410.6765].
V. Khachatryan *et al.*, [CMS Collaboration], JHEP **1703** (2017) 156 [arXiv:1609.05331].

[6] P.A. Baikov, K.G. Chetyrkin and J.H. Kühn, JHEP **1410** (2014) 076 [arXiv:1402.6611].

[7] J. Abdallah *et al.* [DELPHI Collaboration], Eur. Phys. J. **C55** (2008) 525 [arXiv:0804.3883].
R. Barate *et al*. [ALEPH Collaboration], Eur. Phys. J. **C18** (2000) 1 [hep-ex/0008013].
G. Abbiendi *et al.* [OPAL Collaboration], Eur. Phys. J. **C21** (2001) 411 [hep-ex/0105046].
A. Brandenburg *et al.*, Phys. Lett. **B468** (1999) 168 [hep-ph/9905495].
J. Abdallah *et al.* [DELPHI Collaboration], Eur. Phys. J. **C46** (2006) 569 [hep-ex/0603046].

[8] H. Abramowicz *et al.* [ZEUS Collaboration], JHEP **1409** (2014) 7 [arXiv:1405.6915].

[9] ZEUS collaboration, addendum to [8], unpublished.

[10] A. Gizhko, *Measurement of beauty quark mass at HERA and impact on Higgs production in association with beauty quarks*, DESY-THESIS-2016-015.

[11] O. Behnke, A. Geiser, M. Lisovyi, Prog. Part. Nucl. Phys. **84** (2015) 1 [arXiv:1506.07519].

[12] J. Beringer *et al.* [Particle Data Group], Phys. Rev. **D86** (2012) 1.

[13] C. Patrignani *et al.* [Particle Data Group], Chin. Phys. **C40** (2016) 100001.

[14] F.D. Aaron *et al.* [H1 and ZEUS Collaborations], Eur. Phys. J. **C73** (2013) 2311 [arXiv:1211.1182]; and references therein.

[15] S. Alekhin *et al.*, Phys. Lett. **B718** (2012) 550 [arXiv:1209.0436].
S. Alekhin *et al.*, Phys. Lett. **B720** (2013) 172 [arXiv:1212.2355].
S. Alekhin, J. Blümlein, S. Moch, Mod. Phys. Lett. **A28** (2013) 1360018 [arXiv:1307.1219].

[16] J. Gao, M. Guzzi, P.M. Nadolski, Eur. Phys. J. **C73** (2013) 2541 [arXiv:1304.3494].

[17] V. Bertone *et al.* [xFitter Developers' Team Collaboration], JHEP **1608** (2016) 050 [arXiv:1605.01946].

[18] S. Alekhin *et al.*, DESY-16-179, DO-TH-16-13, arXiv:1701.05838.

[19] S. Alekhin, J. Blümlein and S. Moch, Phys. Rev. **D89** (2014) 054028 [arXiv:1310.3059]; and references therein.
For some of the most recent NNLO developments, see also
J. Ablinger *et al.*, Nucl. Phy. **B890** (2014) 48 [arXiv:1409.1135]; Nucl. Phys. **B882** (2014) 263 [arXiv:1402.0359]; Phys. Rev. **D92** (2015) 114005 [arXiv:1508.01449];
A. Behring *et al.*, Eur. Phys. J. **C74** (2014) 3033 [arXiv:1403.6356].

[20] F.D. Aaron *et al.* [H1 and ZEUS Collaboration], JHEP **1001** (2010) 109 [arXiv:0911.0884].

[21] H. Abramowicz *et al.* [H1 and ZEUS Collaboration], Eur. Phys. J. **C75** (2015) 580 [arXiv:1506.06042].

[22] S. Alekhin, `OPENQCDRAD-1.5`, `http://www-zeuthen.desy.de/~alekhin/OPENQCDRAD`.

[23] HERAFitter, `http://herafitter.org`.
M. Botje, Comput. Phys. Commun. **182** (2011) 490 [arXiv:1005.1481].
F. James and M. Roos, Comput. Phys. Commun. **10** (1975) 343.

[24] S. Alekhin *et al.*, Phys. Rev. **D81** (2010) 014032 [arXiv:0908.2766].
S. Alekhin and S. Moch, Phys. Lett. **B699** (2011) 345 [arXiv:1011.5790].

[25] B. Schmidt, M. Steinhauser, Comput. Phys. Commun. **183** (2012) 1845 [arXiv:1201.6149].
K.G. Chetyrkin, J.H. Kühn, M. Steinhauser, Comput. Phys. Commun. **133** (2000) 43 [hep-ph/0004189].

Subset	$N_{\rm dat}$	Q^2 range	μ	$m_c(m_c)$			$m_c(\mu)$	
		[GeV^2]	[GeV]	[GeV]	fit	scale	[GeV]	fit
1	15	2.5–7	3.3	1.256	$^{+0.078}_{-0.070}$	$^{+0.054}_{-0.000}$	0.984	$^{+0.085}_{-0.076}$
2	12	12–18	4.5	1.192	$^{+0.075}_{-0.073}$	$^{+0.043}_{-0.000}$	0.867	$^{+0.077}_{-0.075}$
3	13	32–60	7.0	1.208	$^{+0.092}_{-0.088}$	$^{+0.045}_{-0.000}$	0.830	$^{+0.089}_{-0.085}$
4	7	120–200	12.7	1.344	$^{+0.130}_{-0.131}$	$^{+0.073}_{-0.074}$	0.90	$\pm$ 0.12
5	4	350–650	21.9	1.14	$^{+0.22}_{-0.22}$	$^{+0.13}_{-0.16}$	0.68	$\pm$ 0.19
6	1	2000	44.8	1.05	$^{+0.68}_{-0.76}$	$^{+0.40}_{-0.15}$	0.56	$\pm$ 0.56

Table 1: Values of $m_c(m_c)$ at different scales μ, determined from six different subsets, and corresponding values of $m_c(\mu)$. The first uncertainty (fit) corresponds to the uncertainty $\delta_{\rm fit}^{\rm exp}$ added in quadrature with the symmetrised systematic uncertainties $\delta_1 - \delta_6$. The second uncertainty (scale) of $m_c(m_c)$ corresponds to the scale variation uncertainty δ_7. No scale uncertainty is quoted for $m_c(\mu)$ (see text). The range of Q^2 values contributing to the six data subsets shown in Fig. 1 is given. Also given is the corresponding logarithmic average scale μ for each subset according to Eq. (2), and the number $N_{\rm dat}$ of charm data points contributing to each measurement.

Subset	$\delta_{\rm fit}^{\rm exp}$	δ_1	δ_2	δ_3	δ_4	δ_5	δ_6	δ_7
		(m_b)	(α_s)	(f_s)	(Q_0)	($Q^2_{\rm min}$)	(param.)	(scale)
	[%]	[%]	[%]	[%]	[%]	[%]	[%]	[%]
1	$\pm$ 5.4	$^{+0.1}_{-0.4}$	$^{-1.2}_{+2.6}$	$^{-0.4}_{+0.2}$	+0.5	+1.4	+0.5	$^{+3.1}_{+4.3}$
2	$\pm$ 6.0	$^{+0.2}_{-0.5}$	$^{-0.9}_{+0.7}$	$^{-0.5}_{+0.2}$	+0.3	+1.0	+0.9	$^{+2.4}_{+3.6}$
3	$\pm$ 7.2	$^{+0.3}_{-0.7}$	$^{-0.4}_{+0.3}$	$^{-0.8}_{+0.3}$	+1.7	+0.3	+1.8	$^{+0.1}_{+3.7}$
4	$\pm$ 9.6	$^{+0.5}_{-0.8}$	$^{+0.7}_{-0.6}$	$^{-0.8}_{+0.5}$	+0.5	–1.2	+0.1	$^{-5.5}_{+5.4}$
5	$\pm$ 19.2	$^{+0.5}_{-1.2}$	$^{+1.6}_{-1.8}$	$^{-1.2}_{+0.5}$	–0.5	+2.1	–1.7	$^{-14.3}_{+11.6}$
6	$\pm$ 63.8	$^{-7.4}_{-2.9}$	$^{+5.9}_{-5.7}$	$^{-3.0}_{-7.6}$	+6.5	–33.3	+9.5	$^{+38.1}_{-14.2}$

Table 2: Summary of the systematic uncertainties in the $m_c(m_c)$ determinations. The definitions of the uncertainty sources, the meaning of the symbols in the first and second row and related details are given in the text. In cases where opposite variations of a variable yield uncertainties with the same sign, only the larger one is considered for the uncertainty combination in Table 1. Except for δ_7, these uncertainties also apply to $m_c(\mu)$, before evolution to the appropriate scale.

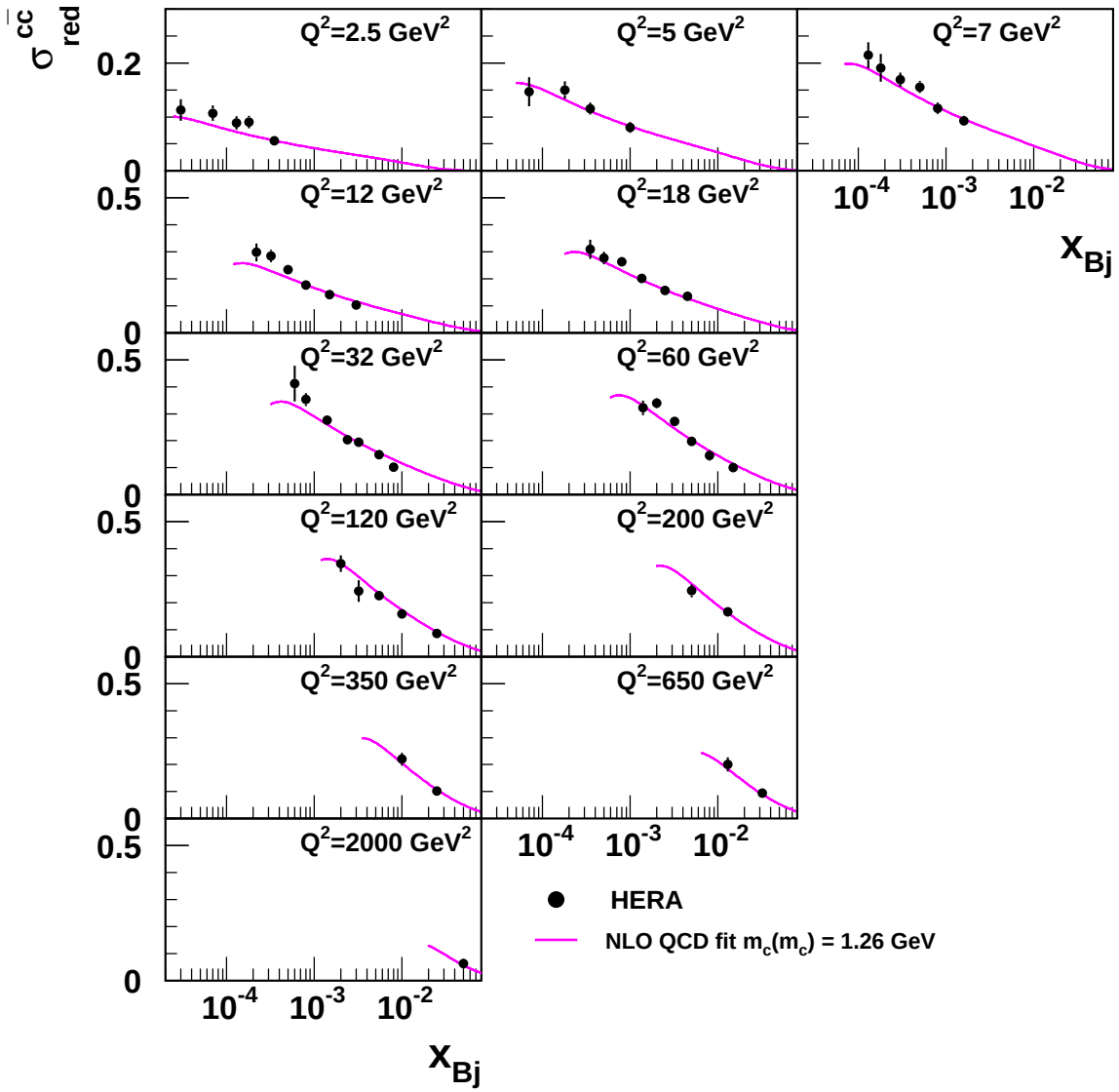

Figure 1: Reduced cross section for charm production in deep-inelastic scattering [14] as a function of the Bjorken scaling variable $x_{\rm Bj}$ for different values of photon virtuality Q^2 (points). The measurements are grouped into six subsets in Q^2, as indicated by the six rows, and detailed in Table 1. The curve shows the global NLO QCD fit for $m_c(m_c) = 1.26$ GeV described in the text.

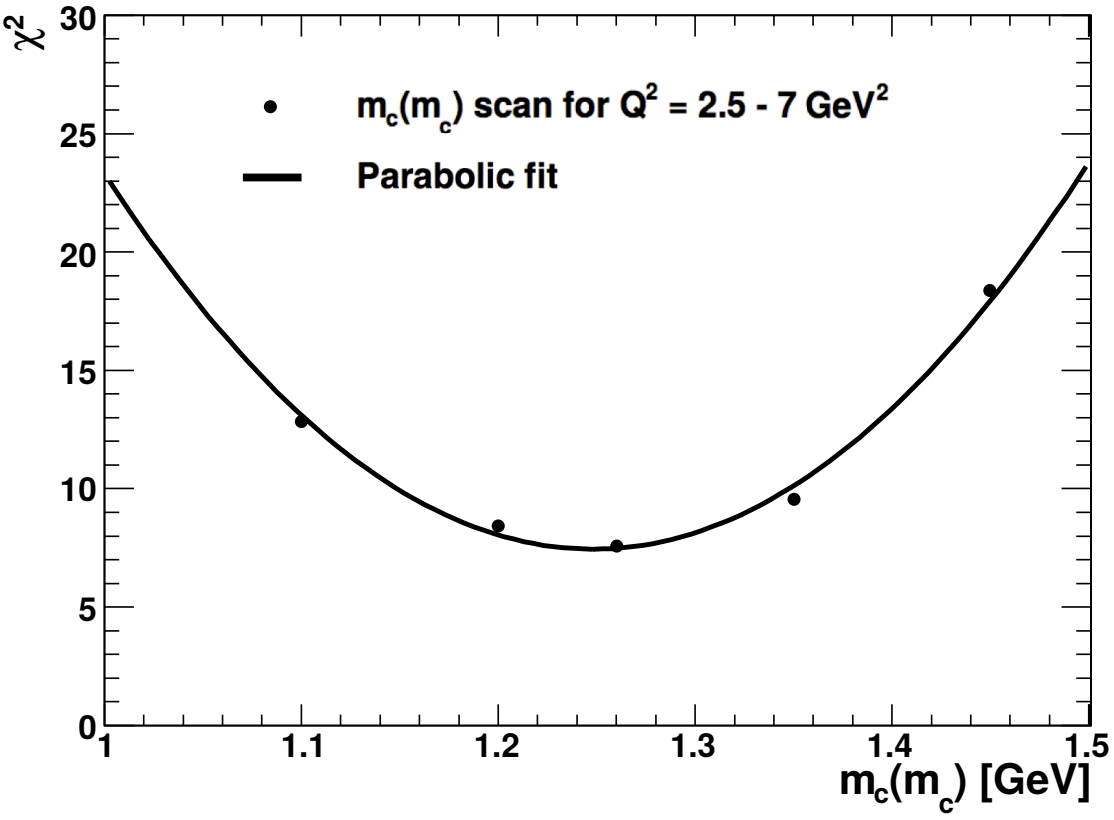

Figure 2: χ^2 of the comparison of the FFNS NLO QCD prediction to the charm reduced cross sections in the first Q^2 interval, $2.5 - 7$ GeV^2, for different values of the charm-quark mass $m_c(m_c)$ in the $\overline{\text{MS}}$ running mass scheme (points). The line shows a parabolic fit.

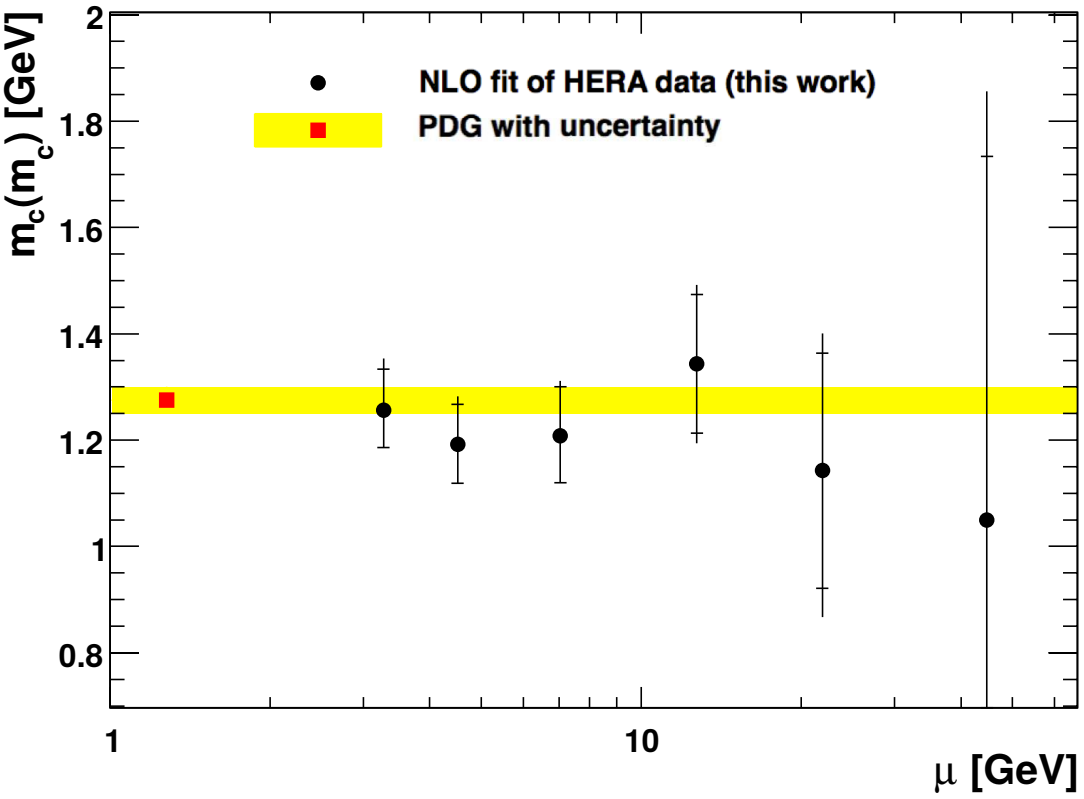

Figure 3: Charm-quark mass $m_c(m_c)$ in the $\overline{\text{MS}}$ running mass scheme determined from the charm data independently at six different scales μ. The outer error bars show the fit uncertainty combined with all model, parametrisation and theoretical systematic uncertainties added in quadrature. The inner error bars show the same uncertainties excluding the uncertainties arising from the variation of the QCD scales. The filled square at scale m_c is the PDG world average [12] and the associated band shows its uncertainty.

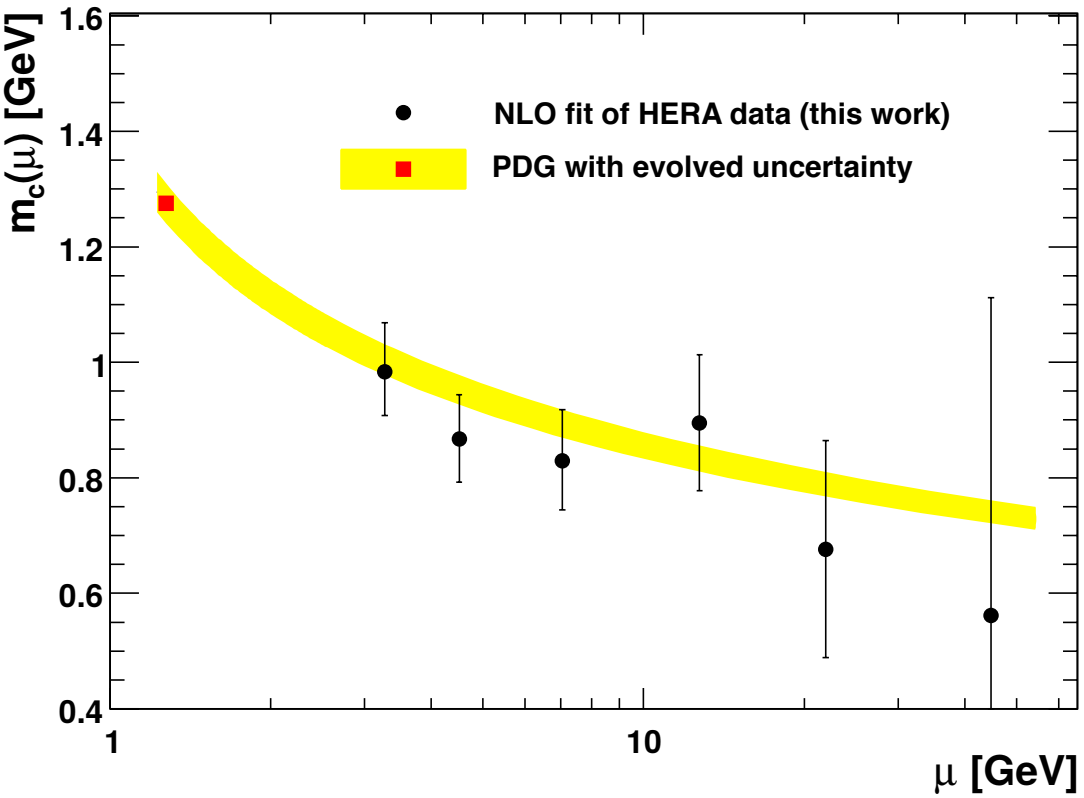

Figure 4: Charm-quark mass $m_c(\mu)$ determined in the $\overline{\text{MS}}$ running mass scheme as a function of the scale μ (black points). The error bars correspond to the inner error bars shown in Fig. 3. The red point at scale m_c is the PDG world average [12] and the band shows the uncertainty and its expected running according to Eq. (3).